Monthly Notices
of the
ROYAL ASTRONOMICAL SOCIETY

Mon. Not. R. Astron. Soc. **403,** 287–294 (2010) doi:10.1111/j.1365-2966.2009.16103.x

Reproducing spacecraft measurements of magnetic correlations in the solar wind

B. Weinhorst and A. Shalchi★

Institut für Theoretische Physik, Lehrstuhl IV: Weltraum- und Astrophysik, Ruhr-Universität Bochum, D-44780 Bochum, Germany

Accepted 2009 November 23. Received 2009 November 18; in original form 2009 October 8

ABSTRACT

Analytical models for magnetic turbulence are an important ingredient in the theory of field line wandering and cosmic ray diffusion. In previous investigations, a so-called *slab*/2D model has been used. In the present article, we develop a more general analytical model for magnetic turbulence. This model is then compared with solar wind observations. We investigate numerically the possibility to explain the *maltese cross* structure of the correlation function of solar wind turbulence with this model.

Key words: magnetic fields – turbulence – solar wind.

1 INTRODUCTION

The solar wind provides a possibility to study magnetohydrodynamic (MHD) turbulence in nature. Since the turbulent magnetic fields $\delta \boldsymbol{B}$ are superposed with a mean magnetic field $\boldsymbol{B}_0 = B_0 \boldsymbol{e}_z$, one expects spectral anisotropy. Here, we have chosen a *Cartesian* system of coordinates so that the z-axis is aligned along the mean field. A similar configuration can be found in the interstellar medium and in other astrophysical scenarios. The turbulent fields can be described by using the magnetic correlation tensor which is also an important input in the analytical and numerical description of field line wandering and charged particle transport (for a review see e.g. Schlickeiser 2002 and Shalchi 2009).

Some properties of the magnetic correlations can be obtained by solar wind observations. Matthaeus, Goldstein & Aaron (1990) discussed measurements by the *ISEE 3 space probe* of the correlation function which shows a *maltese cross* structure when plotted in a two-dimensional (2D) plane where one of the axes is parallel to the mean magnetic field. A simple approximation for this structure is provided by the so-called *two-component model* in which a superposition of pure *slab* modes [with $\delta \boldsymbol{B}(\boldsymbol{x}) = \delta \boldsymbol{B}(z)$] and pure 2D modes [with $\delta \boldsymbol{B}(\boldsymbol{x}) = \delta \boldsymbol{B}(x, y)$] is considered. At least for interplanetary studies, a common assumption is that the magnetic field fluctuations admit a strong component of nearly 2D character comprising perhaps 80–90 per cent of the turbulent inertial-range energy budget (see Bieber, Wanner & Matthaeus 1996). Further measurements were done in the following years (see e.g. Dasso et al. 2005; Osman & Horbury 2007; Horbury, Forman & Oughton 2008; Osman & Horbury 2009a,b) which have confirmed this structure of interplanetary turbulence. More details about the different solar wind observations and the measured *maltese cross* can be found in the two review articles Bruno & Carbone (2005) and Horbury, Forman & Oughton (2005).

Although solar wind observations are the most powerful tool for improving our understanding of turbulence, there was also some remarkable process in the theory of MHD turbulence. Numerical simulations, for instance, suggest that 2D dynamics is the leading order description of turbulence in the presence of a mean magnetic field (see e.g. Oughton, Priest & Matthaeus 1994; Matthaeus et al. 1996). Simulations of incompressible MHD were also performed more recently (e.g. Shaikh & Zank 2007; Dmitruk & Matthaeus 2009). In addition to such numerical studies, there were also some analytical attempts to describe turbulence in the solar wind. The theory of nearly incompressible MHD, for instance, predicts a collapse in dimensionality making turbulence in the solar wind a superposition of a dominant 2D and a slab component (see Zank & Matthaeus 1993). In the latter work, it has been shown that there exist three distinct nearly incompressible descriptions corresponding to different values of the plasma beta β (β is the ratio of thermal to magnetic pressure). In the $\beta \gg 1$ regime, the compressible MHD description converges in the low-Mach-number limit to the equations of classical incompressible three-dimensional (3D) MHD. However, for the remaining plasma beta regimes, the imposition of a large magnetic field forces the equations of fully compressible 3D MHD to converge to the equations of 2D incompressible MHD in the low-Mach-number limit. The *collapse in dimensionality* corresponding to the different plasma beta regimes clarifies the distinction between the 3D and 2D incompressible MHD descriptions. The collapse in dimensionality that occurs as a result of a decreased plasma beta can carry over to the weakly compressible corrections. For $\beta \approx 1$ plasma, Alfvén waves propagate parallel to the applied magnetic field, while for a $\beta \ll 1$ magnetofluid quasi-1D long-wavelength acoustic modes propagate parallel to the applied magnetic field. Hunana, Zank & Shaikh (2006) extend the theory of nearly incompressible hydrodynamics to flows, which include large-scale inhomogeneities.

★E-mail: andreasm4@yahoo.com

Because of these observational, numerical and analytical hints, we conclude that the turbulent field can be well approximated by the two-component model in which we have $\delta \boldsymbol{B}(\boldsymbol{x}) = \delta \boldsymbol{B}(z) + \delta \boldsymbol{B}(x, y)$. In the literature, this model is also known as *slab*/2D composite model.

A further important ingredient in the correlation tensor is the form of the turbulence spectrum. Here one has to distinguish between the large turbulence scales (the so-called energy range of the spectrum), the intermediate scales (inertial range) and the small scales (dissipation range). Whereas the most numerical and observational studies concentrated on the inertial range of the spectrum, the energy range as well as the dissipation range are important for understanding the propagation of cosmic rays (for a review, see e.g. Shalchi 2009). Previously, we have already improved the analytical model for the turbulence spectrum and have studied the influence of large turbulence scales on field line wandering (see Shalchi & Weinhorst 2009), perpendicular diffusion of cosmic rays (see Shalchi, Li & Zank 2009) and the mechanism of particle acceleration at interplanetary shock waves (see Shalchi et al. 2009; Dosch & Shalchi 2009). All these investigations were done by assuming *two-component* turbulence. In order to improve the description of field lines and theories of cosmic ray transport, it is necessary to introduce a more detailed model of the correlation function of the turbulent magnetic fields.

It is the purpose of the present article to replace the standard *two-component* model by a more general model. This model is formulated analytically and is then compared with previous models and solar wind observations. By performing a parameter study, we show how the observed *maltese cross* structure in the solar wind can be reproduced. The analytical model presented in this paper together with the parameter study will allow the improvement of our understanding and the description of transport of field lines and charged particles such as cosmic rays.

The paper is structured as follows. In Section 2, we present the turbulence model used throughout the present article. Section 3 includes a short discussion of the measurements as well as a parameter study of the model. In Section 4, we summarize and conclude in Section 5.

2 THE ANISOTROPIC TURBULENCE MODEL

Magnetic correlation functions, field line mean square displacements and cosmic ray diffusion coefficients are controlled by the turbulence correlation tensor $P_{lm}(\boldsymbol{k}) = \langle \delta B_l(\boldsymbol{k}) \delta B_m^*(\boldsymbol{k}) \rangle$. According to Matthaeus & Smith (1981), the general form of this tensor for axisymmetric turbulence is

$$P_{lm}(\boldsymbol{k}) = A(k_\parallel, k_\perp) \left[\delta_{lm} - \frac{k_l k_m}{k^2} \right], \tag{1}$$

where magnetic helicity has been neglected. In the current article, we employ spherical coordinates with

$$\begin{aligned} k_x &= k_\perp \cos(\Psi) = \sqrt{1-\eta^2} k \cos(\Psi) \\ k_y &= k_\perp \sin(\Psi) = \sqrt{1-\eta^2} k \sin(\Psi) \\ k_z &= k_\parallel = \eta k. \end{aligned} \tag{2}$$

For the function $A(k_\parallel, k_\perp)$, we use in spherical coordinates

$$A(k_\parallel, k_\perp) = \frac{G(k, \eta)}{8\pi k^2} \tag{3}$$

and for the function $G(k, \eta)$ we employ the *Ansatz*

$$G(k, \eta) = l \delta B^2 g(k, l) a(\eta, \Lambda). \tag{4}$$

Table 1. Asymptotic limits of the parameter $a_0(\Lambda)$.

Λ	$a_0(\Lambda)$	Turbulence geometry
$\Lambda \ll 1$	$\frac{2}{\sqrt{\pi\Lambda}}$	2D
$\Lambda = 1$	e	Isotropic
$\Lambda \gg 1$	$2\,\Lambda$	Slab

Here, l denotes a characteristic length-scale of the turbulence (bendover or turnover scale), δB^2 is the total magnetic energy density, $g(k, l)$ is the turbulence wave spectrum and $a(\eta, \Lambda)$ is the anisotropy function. The latter two functions are determined in the following paragraphs. The anisotropy function is chosen so that

$$\frac{1}{2} \int_{-1}^{+1} \mathrm{d}\eta \; a(\eta, \Lambda) = 1. \tag{5}$$

The total spectrum has to fulfil the normalization constraint

$$\delta B^2 \equiv \int \mathrm{d}^3 k \sum_{n=x,y,z} P_{nn}(\boldsymbol{k}). \tag{6}$$

With equations (1), (3) and (4), this becomes

$$\begin{aligned} \delta B^2 &= 2 \int \mathrm{d}^3 k \; A(k_\parallel, k_\perp) = \frac{1}{4\pi} \int \mathrm{d}^3 k \; k^{-2} G(k, \eta) \\ &= \frac{l \delta B^2}{2} \int_{-1}^{+1} \mathrm{d}\eta \; a(\eta, \Lambda) \int_0^\infty \mathrm{d}k \; g(k, l) \\ &= l \delta B^2 \int_0^\infty \mathrm{d}k \; g(k, l). \end{aligned} \tag{7}$$

In the following two paragraphs, models for the functions $a(\eta, \Lambda)$ and $g(k, l)$ are discussed.

2.1 The anisotropy function $a(\eta, \Lambda)$

For the anisotropy function, we choose the Gaussian model

$$a(\eta, \Lambda) = a_0(\Lambda) \mathrm{e}^{-\Lambda^{-1}\eta^2 - \Lambda(1-\eta^2)}. \tag{8}$$

From the normalization condition of equation (5), it follows

$$a_0(\Lambda) = \frac{2}{\sqrt{\pi}} \frac{\sqrt{\Lambda^{-1} - \Lambda}}{Erf\left(\sqrt{\Lambda^{-1} - \Lambda}\right)} \mathrm{e}^{\Lambda}, \tag{9}$$

where we have used the error function $Erf(z)$. In Table 1, we provide some simplifications of the function $a_0(\Lambda)$ for extreme values of the anisotropy parameter Λ.

To derive these limits, we have used (see e.g. Gradshteyn & Ryzhik 2000)

$$\begin{aligned} Erf(|z| \to 0) &\approx \frac{2}{\sqrt{\pi}} \left[z - \frac{z^3}{3} + \cdots \right] \\ Erf(|z| \to \infty) &\approx 1 - \frac{1}{\sqrt{\pi} z} \mathrm{e}^{-z^2} + \cdots \end{aligned} \tag{10}$$

In the following, we consider three limits to understand the anisotropy function $a(\eta, \Lambda)$ defined in equation (8).

2.1.1 The limit $\Lambda \to 0$: pure 2D turbulence

In the case $\Lambda \to 0$ we have

$$a(\eta, \Lambda \to 0) \approx \frac{2}{\sqrt{\pi\Lambda}} \mathrm{e}^{-\frac{\eta^2}{\Lambda}}, \tag{11}$$

where we have used Table 1. The remaining Gaussian function becomes a delta function $\delta(x)$ for the limit considered here

$$\lim_{\sigma\to 0}\frac{1}{\sqrt{2\pi\sigma}}\mathrm{e}^{-\frac{x^2}{2\sigma}} = \delta(x), \tag{12}$$

and thus

$$a(\eta, \Lambda \to 0) = 2\delta(\eta) \sim \delta(k_\parallel). \tag{13}$$

For very small values of Λ, all the magnetic energy is located in the plane perpendicular to the mean field (x–y plane). This model is usually called the 2D model. From the anisotropic model used in the present paper, we can recover the pure 2D model by choosing the limit $\Lambda \to 0$.

2.1.2 *The case* $\Lambda = 1$*: isotropic turbulence*

For $\Lambda = 1$, we derive

$$a(\eta, \Lambda = 1) = a_0(\Lambda = 1)\mathrm{e}^{-1} \tag{14}$$

and with Table 1 we find

$$a(\eta, \Lambda = 1) = 1. \tag{15}$$

Obviously this case corresponds to isotropic turbulence since $a(\eta, \Lambda = 1)$ does no longer depend on the parameter η.

2.1.3 *The case* $\Lambda \to \infty$*: slab fluctuations*

For $\Lambda \to \infty$, equation (8) becomes

$$a(\eta, \Lambda \to \infty) = a_0(\Lambda)\mathrm{e}^{-\Lambda(1-\eta^2)}. \tag{16}$$

With Table 1, we find

$$a(\eta, \Lambda \to \infty) = 2\Lambda\mathrm{e}^{-\Lambda(1-\eta^2)}. \tag{17}$$

The remaining Gaussian function becomes again a delta function $\delta(x)$ for the limit considered here

$$\lim_{\sigma\to 0}\frac{1}{2\sigma}\mathrm{e}^{-\frac{|x|}{\sigma}} = \delta(x), \tag{18}$$

and thus

$$a(\eta, \Lambda \to \infty) = 4\delta\left(\sqrt{1-\eta^2}\right) \sim \delta(k_\perp). \tag{19}$$

Here, all the magnetic energy is located along the parallel axis. This model is usually called the *slab* model. It can be obtained from the anisotropic model by setting $\Lambda \to \infty$. In Figs 1 and 2, the properties of the anisotropy function $a(\eta, \Lambda)$ are shown for different values of Λ.

In principle, one could consider a superposition of two anisotropic models with different Λ's. For instance, we can superpose an anisotropic model with $\Lambda = 0.1$ (2D like) and a model with $\Lambda = 10$ (*slab* like). In this case, the contour plot has the form of a *maltese cross*. Such a form can indeed be observed in the solar wind (see Matthaeus et al. 1990). In Section 2.3, we discuss such a superposition of two anisotropic models and in Section 3 we compare the correlations with solar wind observations.

2.2 The turbulence wave spectrum $g(k, l)$

For a complete description of the turbulence, we also have to specify the k-dependence of the correlation tensor and therefore the spectral function $g(k, l)$. Several models have been proposed in the past. A prominent example is the model $g(k, l) = 4C(s)[1 + (lk)^2]^{-s/2}$ (see e.g. Bieber et al. 1994). This spectrum is constant at large

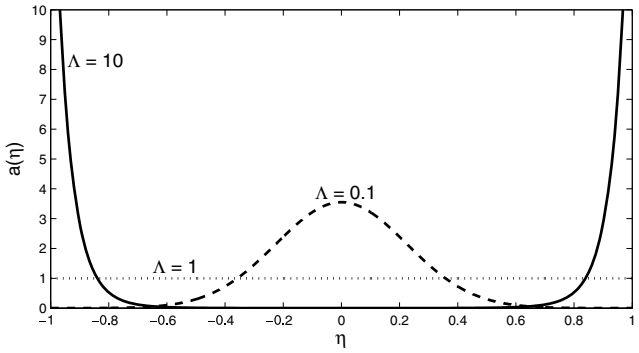

Figure 1. The anisotropy function $a(\eta, \Lambda)$ for different values of the anisotropy parameter Λ. Shown is $a(\eta, \Lambda)$ for $\Lambda = 0.1$ (dashed line), $\Lambda = 1$ (dotted line) and $\Lambda = 10$ (solid line). The first case corresponds to 2D-like fluctuations and the second case to isotropic turbulence, and the third case is equal to *slab*-like fluctuations.

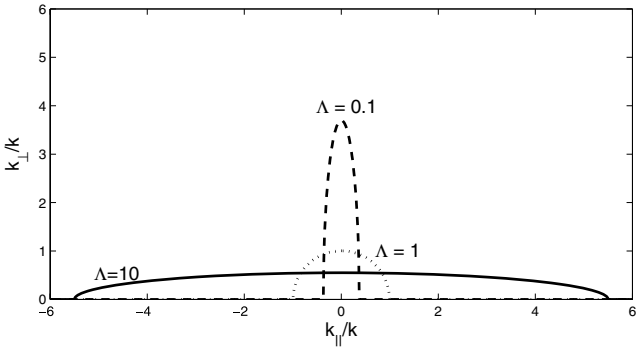

Figure 2. Contour plot of the anisotropy function with $a(\eta, \Lambda) = 1$. Shown is $a(\eta, \Lambda)$ for $\Lambda = 0.1$ (dashed line), $\Lambda = 1$ (dotted line) and $\Lambda = 10$ (solid line). The first case corresponds to 2D-like fluctuations and the second case to isotropic turbulence, and the third case is equal to *slab*-like fluctuations.

turbulence scales (energy range) where $k \le l^{-1}$. For small scales (inertial range) where $k \ge l^{-1}$, we find a decreasing spectrum with the inertial-range spectral index s. In the literature, several values for s have been proposed such as the value $s = 5/3$ proposed by Kolmogorov (1941) or $s = 3/2$ proposed by Kraichnan (1965).

In the present article, we use the more general form of the spectrum introduced by Shalchi & Weinhorst (2009)

$$g(k, l) = C(s, q)\frac{|kl|^q}{[1 + (kl)^2]^{(s+q)/2}}. \tag{20}$$

For the normalization constant $C(s, q)$, we have

$$C(s, q) = \frac{2\Gamma\left(\frac{s+q}{2}\right)}{\Gamma\left(\frac{s-1}{2}\right)\Gamma\left(\frac{q+1}{2}\right)}. \tag{21}$$

The spectrum is correctly normalized for $s > 1$ and $q > -1$. The spectrum is decreasing in the inertial range ($k \ge l^{-1}$) where the spectrum has the form $\sim k^{-s}$. We can reproduce an increasing (positive q) and decreasing (negative q) spectrum in the energy range ($k < l^{-1}$).

2.3 The superpositioned anisotropy model

In the previous paragraphs, we have described the magnetic correlation tensor $P_{lm}(\boldsymbol{k})$ which describes the magnetic correlations in the wave-vector space. The magnetic correlation tensor in the real

space $R_{lm}(\boldsymbol{x})$ is linked to this tensor via a *Fourier transformation*

$$R_{lm}(\boldsymbol{x}) = \int \mathrm{d}^3k \; P_{lm}(\boldsymbol{k})\mathrm{e}^{\mathrm{i}\boldsymbol{k}\cdot\boldsymbol{x}}. \tag{22}$$

Solar wind turbulence may be described by a superposition of two anisotropic models with different Λ's. We define the superpositioned anisotropy model by

$$\begin{aligned} R(z,r) &\equiv aR^{\mathrm{2D}}(z,r) + (1-a)R^{slab}(z,r) \\ &= \int \mathrm{d}^3k \; \Bigg[a \sum_{n=x,y,z} P_{nn}^{\mathrm{2D}}(\boldsymbol{k}) \\ &\quad + (1-a) \sum_{n=x,y,z} P_{nn}^{slab}(\boldsymbol{k}) \Bigg] \mathrm{e}^{\mathrm{i}\boldsymbol{k}\boldsymbol{x}}. \end{aligned} \tag{23}$$

Here a defines the percentage of 2D corresponding turbulence from the original fluctuation. In the original *two-component* model, the tensor $P_{nm}^{slab}(\boldsymbol{k})$ describes the *slab* fluctuations and $P_{nm}^{\mathrm{2D}}(\boldsymbol{k})$ the 2D modes. In the present paper, we replace these two tensor components by the model described in the previous sections.

With equation (2) and

$$x = r\cos(\phi), \quad y = r\sin(\phi), \quad z = z, \tag{24}$$

we find

$$\boldsymbol{k}\boldsymbol{x} = kr\sqrt{1-\eta^2}\cos(\Psi-\phi) + \eta kz. \tag{25}$$

Therefore, equation (23) can be written as

$$\begin{aligned} R(z,r) = \int_0^\infty \mathrm{d}k \int_{-1}^{+1} \mathrm{d}\eta \; \Bigg[& a \sum_{n=x,y,z} P_{nn}^{\mathrm{2D}}(\boldsymbol{k}) \\ & + (1-a) \sum_{n=x,y,z} P_{nn}^{slab}(\boldsymbol{k}) \Bigg] \\ & \times \int_0^{2\pi} \mathrm{d}\Psi \; \mathrm{e}^{\mathrm{i}kr\sqrt{1-\eta^2}\cos(\Psi-\phi)+i\eta kz}. \end{aligned} \tag{26}$$

After P_{xx}, P_{yy} and P_{zz} do not depend on Ψ, we can solve the Ψ-integration in equation (23) by using Gradshteyn & Ryzhik (2000). We find

$$\begin{aligned} R(z,r) = \int_0^\infty \mathrm{d}k \int_{-1}^{+1} \mathrm{d}\eta \; \Bigg[& a \sum_{n=x,y,z} P_{nn}^{\mathrm{2D}}(\boldsymbol{k}) \\ & + (1-a) \sum_{n=x,y,z} P_{nn}^{slab}(\boldsymbol{k}) \Bigg] \\ & \times 2\pi J_0\left(kr\sqrt{1-\eta^2}\right)\cos(\eta kz), \end{aligned} \tag{27}$$

where we used the independence of the phase shift ϕ and calculated the real part of $R(z,r)$. With equations (1), (3) and (4) and using the anisotropy function $a(\eta,\Lambda)$ defined in equation (8) as well as the turbulence wave spectrum $g(k,l)$ (see equation 20), we find

$$\begin{aligned} R(z,r) = {} & \frac{1}{2}\delta B^2 \int_0^\infty \mathrm{d}k \int_{-1}^{1} \mathrm{d}\eta \; J_0\left(kr\sqrt{1-\eta^2}\right)\cos(\eta kz) \\ & \times \Bigg\{ a \Bigg[a_0(\Lambda_{\mathrm{2D}})\mathrm{e}^{-\Lambda_{\mathrm{2D}}^{-1}\eta^2-\Lambda_{\mathrm{2D}}(1-\eta^2)} l_{\mathrm{2D}} C(s_{\mathrm{2D}}, q_{\mathrm{2D}}) \\ & \times \frac{|kl_{\mathrm{2D}}|^{q_{\mathrm{2D}}}}{\left(1+l_{\mathrm{2D}}^2k^2\right)^{\frac{s_{\mathrm{2D}}+q_{\mathrm{2D}}}{2}}} \Bigg] \\ & + (1-a) \Bigg[a_0(\Lambda_{slab})\mathrm{e}^{-\Lambda_{slab}^{-1}\eta^2-\Lambda_{slab}(1-\eta^2)} l_{slab} C(s_{slab}, q_{slab}) \\ & \times \frac{|kl_{slab}|^{q_{slab}}}{(1+l_{slab}^2k^2)^{\frac{s_{slab}+q_{slab}}{2}}} \Bigg] \Bigg\}. \end{aligned} \tag{28}$$

This model depends on nine parameters, these are a, Λ_{slab}, l_{slab}, s_{slab}, q_{slab}, Λ_{2D}, l_{2D}, s_{2D} and q_{2D}. In the next section, we will show how each of these parameters influences $R(z,r)$.

3 PARAMETER STUDY AND COMPARISON WITH OBSERVATIONS

3.1 Solar wind measurements

Matthaeus et al. (1990) published data on the fluctuations of the solar magnetic field. Fig. 6 (left-hand panel) shows a contour plot of the 2D correlation function of solar wind fluctuations as a function of distance parallel and perpendicular to the mean magnetic field. The four-quadrant plot is produced by reflecting the data across the axes from the first quadrant. Matthaeus et al. interpreted the contours elongated parallel to $r = r_\perp$ as Alfvén waves with $\boldsymbol{k} \| \boldsymbol{B}_0$ and the contours elongated parallel to $z = r_\parallel$ as fluctuations in the 2D turbulence. At small separations, z, $r \leq 5 \times 10^{10}$ cm *slab* symmetry appears dominant, whereas contributions from a quasi-2D component become very noticeable for z, $r \geq 15 \times 10^{10}$ cm.

From their paper, one can deduce that the correlation function decreases to about 40 per cent along the axis, with the 2D component a little smaller than the *slab* component, and to about 30 per cent along the bisectrix. With the 2D symmetry dominating the contours, thus on large scales, the contours become more aligned to the bisectrix. Along the axis, the correlation function decreases faster than along a line separated from the former by an angle of approximately 10°. Furthermore, the correlation does seem to decline slower then exponentially, nearly linear. By reflecting the data from the first quadrant across the axes a four-quadrant plot is obtained, which resembles a *maltese cross* contour.

3.2 The standard *slab*/2D model

Here, we explore the magnetic correlations by using the standard *slab*/2D model. To calculate the correlation function plotted in Fig. 3 (left-hand panel), we used the limits of equations (13) and (19) and choose $q = q_{\mathrm{2D}} = q_{slab} = 0$ to get the turbulence spectrum used, e.g., by Bieber et al. (1994). For this plot, an 80 per cent 2D to 20 per cent *slab*-energy distribution with $s = 5/3$ for the spectral index and $l_{\mathrm{2D}} = 0.003$ au $\approx 4.488 \times 10^{10}$ km and $l_{slab} = 0.03$ au $\approx 44.88 \times 10^{10}$ km as the bendover scales has been assumed. These values of the parameters are most often used throughout the literature. The 2D component dominates for small scales and the *slab* component becomes noticeable for large scales. Therefore, in order to reproduce the measurement, it will be necessary to choose $l_{\mathrm{2D}} > l_{slab}$ and more than 50 per cent *slab* in the energy distribution. Additionally, the correlation declines along the axis only to the starting value of the turbulence, thus along the z-axes to 0.8 (2D turbulence) and along the r-axes to 0.2 (*slab* turbulence). Furthermore, there is no alignment with the bisectrix. These flaws cannot be corrected within this model by changing the parameters.

The next step is to implement the more general form of the power spectra, thus choosing $q \neq 0$. In the literature, one finds $q_{slab} = 0$ and $q_{\mathrm{2D}} \neq 0$, thus we choose $q_{\mathrm{2D}} = 2$ in order to get a finite correlation length (see Matthaeus et al. 2007). The result is illustrated in Fig. 3 (right-hand panel). Of course, again, the 2D component dominates for small scales and the *slab* component becomes noticeable for large scales. A difference with respect to the first plot is the faster decline of the correlation, mainly for the contours corresponding to 2D-like turbulence. On the other hand, one can see an alignment with the bisectrix of the contours elongated along the z-axes. This

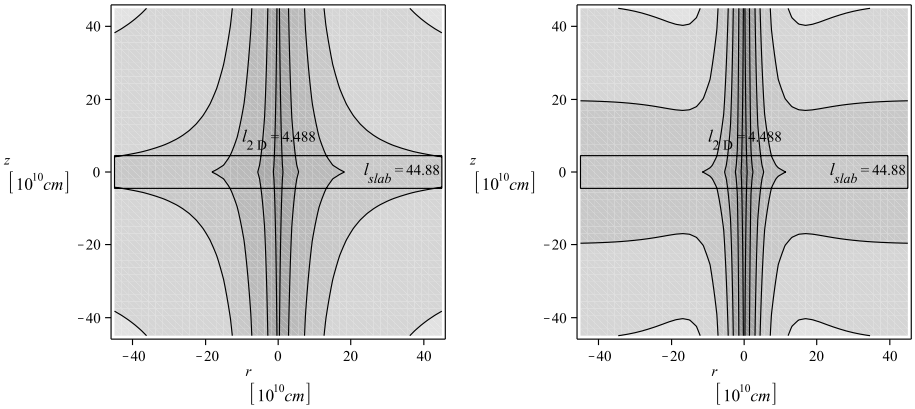

Figure 3. Left-hand panel: correlation function of the standard *slab*/2D model with the standard wave spectrum used, e.g., by Bieber et al. (1994). Right-hand panel: correlation function of the *slab*/2D model now with the more general form of the wave spectrum introduced by Shalchi & Weinhorst (2009). For the full parameter sets see Table 2.

Table 2. Parameter study for $R(z, r)$. The values in bold are the standard values used for our calculations.

Figure	a	l_{2D} (au)	l_{slab} (au)	Λ_{2D}	Λ_{slab}	q_{2D}	q_{slab}
3 (l)	0.8	0.003	0.03	N/A	n/a	0	0
3 (r)	0.8	0.003	0.03	N/A	n/a	2	0
4 (1)	0.4	0.01	0.006	0.1	10	0.5	2
4 (2)	**0.6**	0.01	0.006	0.1	10	0.5	2
4 (3)	0.4	**0.03**	0.006	0.1	10	0.5	2
4 (4)	0.4	0.01	**0.01**	0.1	10	0.5	2
4 (5)	0.4	0.01	0.006	**0.01**	10	0.5	2
4 (6)	0.4	0.01	0.006	0.1	**50**	0.5	2
4 (7)	0.4	0.01	0.006	0.1	10	**2**	2
4 (8)	0.4	0.01	0.006	0.1	10	0.5	**0.5**
5 (l)	0.8	0.003	0.03	0.1	10	0	0
5 (r)	0.8	0.003	0.03	0.1	10	2	0
6 (r)	0.4	0.03	0.01	0.1	30	0.5	2

alignment may be increased by changing the parameters, but still the correlation declines along the axis only to the starting values for the corresponding turbulence.

3.3 Parameter study

In the following, we perform a parameter study for our superpositioned anisotropy model to describe how changing one parameter changes the correlation function $R(z, r)$. Table 2 gives the chosen parameter for each plot in Fig. 4. Plot (1) of Fig. 4 (number in the upper-left corner of each plot) is the reference plot with the following set of parameters:

$a = 0.4, \quad l_{2D} = 0.01\,\text{au}, \quad l_{slab} = 0.006\,\text{au}, \quad \Lambda_{2D} = 0.1,$
$\Lambda_{slab} = 10, \quad q_{2D} = 0.5, \quad q_{slab} = 2, \quad s_{2D} = s_{slab} = 5/3.$

Plots (2) to (8) show the change of $R(z, r)$ with respect to plot (1) due to varying one parameter. For better comparison, we stick to the following contours for each plot $R(z, r) = -0.03, -0.01, 0.01, 0.05, 0.1, 0.2, 0.3, 0.5, 0.8$. On the horizontal and vertical axis r and z are given, respectively, in units of 10^{10} cm. In order to illustrate the involved scales, we show in each plot a rectangle that displays the *slab* and 2D bendover scale used for the calculations. Here l is also given in units of 10^{10} cm.

Before we start to compare the plots (2)–(8) with plot (1), we want to discuss the latter a little further. The plot results from the sum of the two correlation functions R^{2D} and R^{slab}, which differ in the anisotropy function $a(\Lambda)$ plotted in Fig. 2. As expected, the cross-like structure reappears in the plots of $R(z, r)$ (Fig. 4). The contours do not exactly resemble ellipses but an hourglass, thus becoming more narrow in the middle (due to $q > 0$). Due to this, the contours seem to align with the bisectrix. In contrast to the standard *slab*/2D model, we find the correlation function to decline along the axis to very small values. We choose the parameter set for the reference plot as given above in order to best illustrate the influence of each parameter and to show an intermediate step between the commonly used parameter set (see Fig. 5) and the set that best reproduces the measurement (see Fig. 6).

For $a = 0.4$, the fluctuations are 60 per cent *slab* and 40 per cent 2D like; this results in the domination of *slab* symmetry for small scales. After $l_{2D} > l_{slab}$, one finds 2D symmetry to be very noticeable for larger scales. The outcome of changing parameter a from 0.4 to 0.6 [compare plots (1) and (2)] is that the 2D component is dominant for large scales and of the same order as the *slab* component at small scales.

We continue the parameter study by changing l_{2D} from 0.01 au $\approx 14.96 \times 10^{10}$ cm to 0.03 au $\approx 44.88 \times 10^{10}$ cm [compare plots (1) and (3)]. Clearly, a change in the amplitude of the correlation function $R(z, r)$ can be seen. However, the increase is not restricted to the 2D fluctuations but can also be seen in the contours elongated parallel to the horizontal axis corresponding to *slab*-like fluctuations. Comparing this to the effect introduced by changing l_{slab} from 0.006 au $\approx 8.98 \times 10^{10}$ cm to 0.01 au $\approx 14.96 \times 10^{10}$ cm [compare plots (1) and (4)], one can see that only the horizontal contours (*slab*) become bigger, the 2D-like vertical contours even shrink some amount.

Manipulating the anisotropy more towards pure *slab*-like or pure 2D-like fluctuations by increasing Λ_{slab} or decreasing Λ_{2D} ($\Lambda = 1$ corresponds to isotropic fluctuations) results in the plots (5) and (6) of Fig. 4. One can see that by increasing the anisotropy, one gets thinner but longer elliptical contours parallel to the z- and r-axis corresponding to 2D- and *slab*-like fluctuations, respectively. Interestingly the contours of the 2D fluctuations become more *diagonal* if one increases the *slab* anisotropy parameter Λ_{slab}. This is not the case if one decreases Λ_{2D}, neither for the 2D nor the *slab* contours.

In the following, we study the influence of the energy-range spectral index q. For this compare plot (1) with plot (7) for q_{2D} and (8) for q_{slab}. In the first case, q_{2D} is changed from its initial value 0.5 to 2. This effects the correlation function such that both

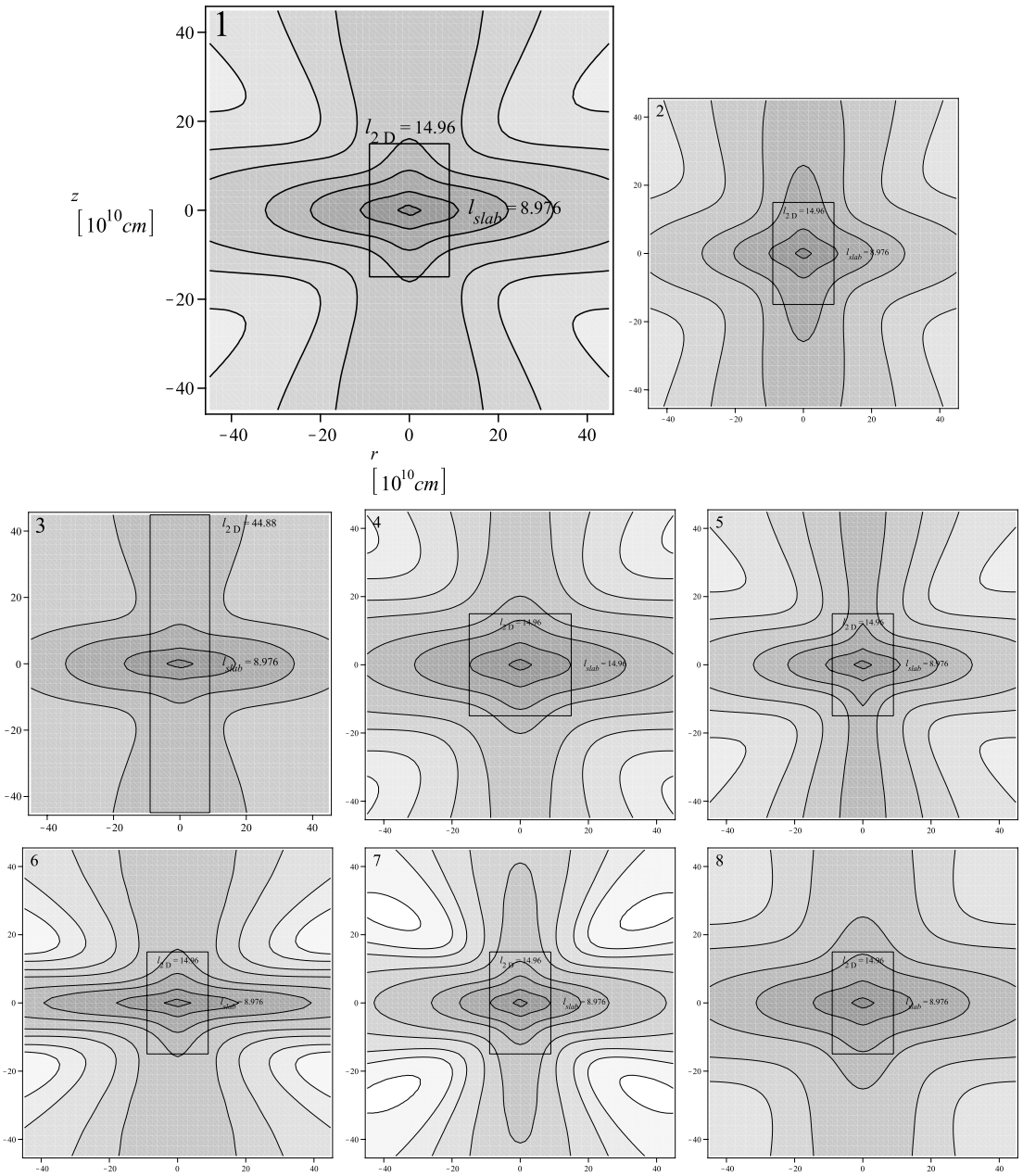

Figure 4. Parameter study for the superpositioned anisotropy model. Shown is the correlation function R in the z, r-plane, units in 10^{10} cm. Grey shading and contours remain the same throughout all plots. The box displays the 2D and *slab* bendover scale, also in 10^{10} cm. Plot (1) is the reference plot, whereas one parameter has been changed for the plots (2)–(8) with respect to plot (1). The following parameters have been changed for the given plot – (2): a, (3): l_{2D}, (4): l_{slab}, (5): Λ_{2D}, (6): Λ_{slab}, (7): q_{2D} and (8): q_{slab} (see Table 2 for details).

elliptical contours become smaller, thus decreasing the overall amplitude of $R(z, r)$. However, the effect is stronger for the 2D correlation. Furthermore, the gradient in the diagonal direction gets steeper which introduces contours in a more *maltese-like cross*. Changing q_{slab} from 2 to 0.5 amplifies the correlation of the *slab*-like fluctuations but also makes the contours more cross like, thus less *maltese cross* like. We also played with the inertial-range spectral index but found that the measurement is consistent with $s = s_{2D} = s_{slab} = 5/3$.

As discussed above, other sets of parameters have been used in previous studies, the left- and right-hand plots of Fig. 5 show the results for $l_{slab} = 0.03$ au, $l_{2D} = 0.003$ au with $q_{slab} = q_{2D} = 0$ and $q_{slab} = 0$, $q_{2D} = 2$, respectively. Comparing these plots with the plots from Fig. 3, one can see the difference between the standard *slab*/2D model and the superpositioned anisotropy model for the given parameter set. The most important difference to the *slab*/2D model discussed in Section 3.2 is the decline of the correlation function along the axis below the starting value of the respective turbulence. The introduction of a positive energy spectral index q again results in an alignment with the bisectrix (Fig. 5, right-hand panel).

3.4 Reproducing the solar wind measurements

We now have some insights into how to change the set of parameters in order to produce a specific kind of plot. The correlation function

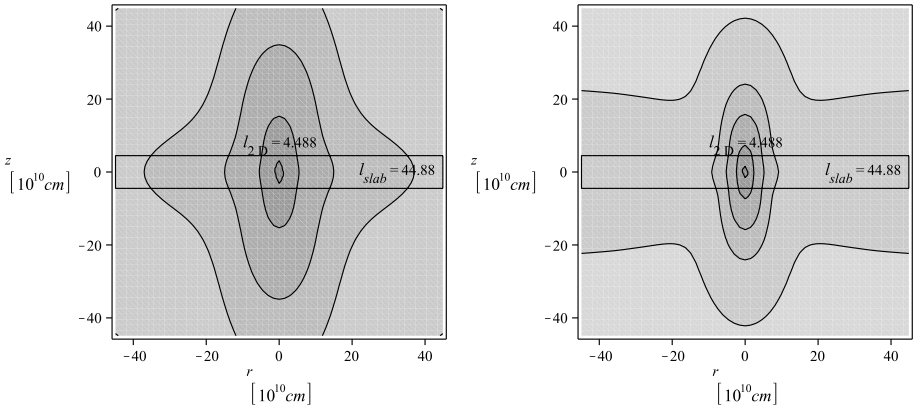

Figure 5. Left-hand panel: correlation function of the superpositioned anisotropy model with the standard wave spectrum with $q = 0$. Right-hand panel: same model but with the more general spectrum introduced by Shalchi & Weinhorst (2009). Compare these plots with Fig. 3 to see the difference between this model and the standard *slab*/2D model. For the full parameter sets see Table 2.

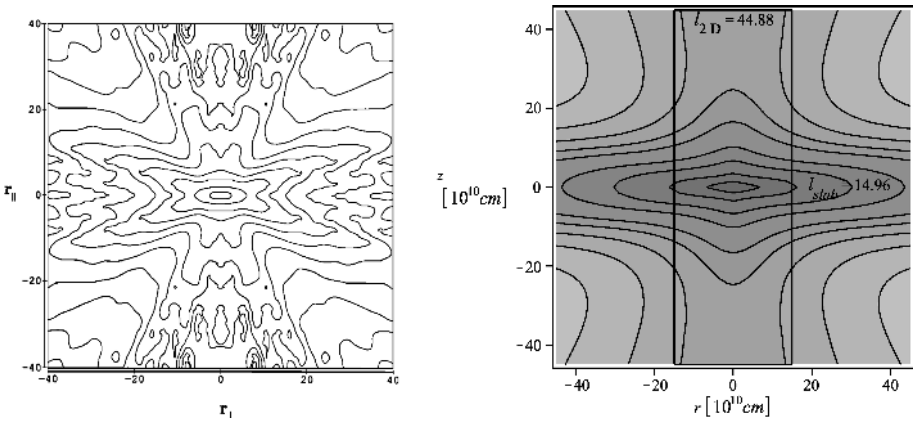

Figure 6. Left-hand panel: Plot taken from Matthaeus et al. (1990). The correlation function for the magnetic fluctuation measurement is plotted. In the notation of this paper $r_\perp = r$ and $r_\parallel = z$. Units in 10^{10} cm. Right-hand panel: this figure shows the plot with the best parameter set estimated from the parameter study shown in Fig. 4. The grey shading displays the same amplitude as in Fig. 4 but we added additional contours. We find quite a good agreement between this plot and the measurements shown on the left.

in the reference plot of Fig. 4 drops along the axis to approximately 10 per cent and along the bisectrix below 1 per cent. Thus, in order to reproduce the measurement the amplitude of the correlation function has to be increased. The effect, that the contours align with the bisectrix for larger z and r, is already sufficient in the reference plot but has to be re-established after increasing the amplitude. A pure *slab*/2D model has non-vanishing spectra only along the $k_\perp$ and $k_\parallel$ axes, and the purpose of our model was to introduce non-vanishing off-axis spectra by substituting the δ function by the anisotropy function $a(\Lambda)$, thus giving elliptical contours (see Fig. 2). Using this anisotropy function, we find the correlation function decline to zero also along the axis, in contrast to the standard *slab*/2D model. With our model, we are now able to reproduce the alignment with the bisectrix as well as the decline of correlation along the axis. However, we have not been able to reproduce the faster decrease along the axis yet.

In order to reproduce the measurement, we chose larger bendover scales l_{2D} and l_{slab} to increase the correlation of the magnetic field fluctuations. Additionally, we enlarge the anisotropy parameter Λ_{slab} in order to maintain the alignment with the bisectrix. The whole set of parameters is also listed in Table 2 and the result is given in Fig. 6. For the plot, we chose the same grey scaling as for the plots of Fig. 4 but additional contours, namely 0.1, 0.15, 0.2, 0.25, 0.3, 0.4, 0.5, 0.65 and 0.8.

Along the axis the correlation drops to 40 per cent at $r = 40 \times 10^{10}$ cm and to 20 per cent at $z = 40 \times 10^{10}$ cm. Along the bisectrix, the correlation decreases to approximately 10 per cent at $z = r = 40 \times 10^{10}$ cm. Although the alignment with the bisectrix is less pronounced than in the reference plot [Fig. 4 (1)], it is still clearly visible.

We think that one may use this model to better estimate the parameters for the correlation of magnetic field fluctuations. Nevertheless, we want to stress that this set of parameters should not be assumed to be a best-fitting parameter set. Primarily, neither do we have the exact values of the correlation function plotted in Fig. 6 (left-hand panel) nor any estimates concerning its error. The purpose of this estimate is only such that we want to demonstrate that it is possible to reproduce this measurement in more details with our model than with the standard *slab*/2D model.

Nevertheless, we like to point out that currently in the literature assumed values of the parameters do not match the measurement of the solar wind magnetic turbulence correlation function discussed here [compare Fig. 6 (left-hand panel) to Figs 3 and 5]. Neither the distribution of 80 per cent 2D and 20 per cent *slab*-like turbulence

nor $l_{slab} > l_{2D}$ can be confirmed by the measurement. The needed cross results from $l_{2D} > l_{slab}$ and a distribution of more *slab* than 2D turbulence. In order to reproduce the *maltese-cross*-like structure, an alignment with the bisectrix as well as decreasing correlation functions along the axis are necessary, thus implying the need for a non-vanishing positive q and preferring the anisotropy model introduced in this article.

4 SUMMARY AND CONCLUSION

Since the knowledge of the magnetic correlation tensor is essential for computing field line diffusion coefficients and the cosmic ray diffusion tensor, we have improved the analytical model for this tensor. We have replaced the standard *two-component* model by a more general form. To do this, we included a parameter Λ which describes the anisotropy. By superposing two anisotropic models we developed a quasi-*two-component* model. In comparison with the original model, our model takes into account the spread of wave vectors around the strict parallel and perpendicular directions.

By combining this model with the general turbulence spectrum proposed by Shalchi & Weinhorst (2009), we were able to reproduce the measurements of the correlation of magnetic turbulence in the solar wind which has the form of a *maltese cross*. Our results match the data much better than any previous work. Up to now our model includes nine parameters, which needs to be fitted by measurements. Although these are a lot of parameters, this study has been able to show the need for spectral anisotropy as well as the more general spectrum in order to explain the structure found for solar wind turbulence.

Additionally, we showed that the standard *slab*/2D model for values of the parameters often used throughout the literature does not agree with the measured magnetic turbulence correlation function. Thus, an additional study of further measurements is required to fully understand the solar wind magnetic properties. The model developed here could be the basis for future investigations of field line and cosmic ray transport.

ACKNOWLEDGMENTS

This research was supported by Deutsche Forschungsgemeinschaft (DFG) under the Emmy-Noether programme (grant SH 93/3-1). As a member of the *Junges Kolleg,* AS also acknowledges support by the Nordrhein-Westfälische Akademie der Wissenschaften.

REFERENCES

Bieber J. W., Matthaeus W. H., Smith C. W., Wanner W., Kallenrode M.-B., Wibberenz G., 1994, ApJ, 420, 294
Bieber J. W., Wanner W., Matthaeus W. H., 1996, J. Geophys. Res., 101, 2511
Bruno R., Carbone V., 2005, Living Rev. Sol. Phys., 2, 4
Dasso S., Milano L., Matthaeus W., Smith C., 2005, ApJ, 635, L181
Dmitruk P., Matthaeus W. H., 2009, Phys. Plasmas, 16, 062304
Dosch A., Shalchi A., 2009, Adv. Space Res., submitted
Gradshteyn I. S., Ryzhik I. M., 2000, Table of Integrals, Series, and Products. Academic Press, New York
Horbury T. S., Forman M. A., Oughton S., 2005, Plasma Phys. Controlled Fusion, 47, B703
Horbury T., Forman M., Oughton S., 2008, Phys. Rev. Lett., 101, 175005
Hunana P., Zank G. P., Shaikh D., 2006, Phys. Rev. E, 74, 026302
Kolmogorov A. N., 1941, Dokl. Akad. Nauk. SSSR, 30, 301
Kraichnan R., 1965, Phys. Fluids, 8, 1835
Matthaeus W. H., Smith C., 1981, Phys. Rev. A - Gen. Phys., 24, 2135
Matthaeus W. H., Goldstein M. L., Aaron R. D., 1990, J. Geophys. Res., 95, 20673
Matthaeus W. H., Ghosh S., Oughton S., Roberts D., 1996, J. Geophys. Res., 101, 7619
Matthaeus W. H., Bieber J. W., Ruffolo D., Chuychai P., Minnie J., 2007, ApJ, 667, 956
Osman K. T., Horbury T. S., 2007, ApJ, 654, L103
Osman K. T., Horbury T. S., 2009a, J. Geophys. Res., 114, A06103
Osman K. T., Horbury T. S., 2009b, Ann. Geophys., 27, 3019
Oughton S., Priest E., Matthaeus W. H., 1994, J. Fluid Mech., 280, 95
Schlickeiser R., 2002, Cosmic Ray Astrophysics. Springer, Berlin
Shaikh D., Zank G. P., 2007, ApJ, 656, L17
Shalchi A., 2009, Non-linear Cosmic Ray Diffusion Theories. Astrophysics and Space Science Library, Vol. 362. Springer, Berlin
Shalchi A., Weinhorst B., 2009, Adv. Space Res., 43, 1429
Shalchi A., Li G., Zank G. P., 2009, Ap&SS, 325, 99
Zank G. P., Matthaeus W. H., 1993, Phys. Fluids A, 5, 257

This paper has been typeset from a TEX/LATEX file prepared by the author.